Article

Evaluation of Benzene Adsorption onto Grass-Derived Biochar and Comparison of Adsorption Capacity via RSM (Response Surface Methodology)

Yuhyeon Na [1,†], Seung Hyeon Weon [1,†], Gyu-Won Lee [1], Hyung Joo Kim [1], Sang Hyun Lee [1], Young-Hoo Kim [1,2], Ji Eun Kim [3], Gwangnam Kang [3], Saerom Park [2,*] and Yong-Keun Choi [1,2,*]

1   Department of Biological Engineering, Konkuk University, Seoul 05029, Republic of Korea;
    yuh.na24@gmail.com (Y.N.); shweon99@gmail.com (S.H.W.); unimosgw@naver.com (G.-W.L.);
    hyungkim@konkuk.ac.kr (H.J.K.); sanghlee@konkuk.ac.kr (S.H.L.); imgz1215@gmail.com (Y.-H.K.)
2   R&D Center, Choilab Inc., Seoul 01811, Republic of Korea
3   R&D Center, ATE Corporation, Seoul 05029, Republic of Korea; jekim@atecorp.co.kr (J.E.K.);
    gnkang@atecorp.co.kr (G.K.)
*   Correspondence: angel4y@naver.com (S.P.); dragonrt@konkuk.ac.kr (Y.-K.C.); Tel.: +82-10-4038-4656 (S.P.);
    +82-02-450-3517 (Y.-K.C.)
†   These authors contributed equally to this work.

Abstract: The present study reports the effective removal of benzene in aqueous phase onto biochar. The adsorption capacity of benzene onto biochars made at different pyrolytic temperatures (e.g., 350, 550, and 750 °C) and from various feedstocks (e.g., grape pomace, rice husk, and Kentucky bluegrass) were investigated. The adsorption capacity of Kentucky bluegrass-derived biochar (KB-BC) prepared at 550 °C for benzene was better than other biochars, owing to the higher surface area and functional groups. The adsorption isotherms and kinetics model for benzene by KB-BC550 fitted the Freundlich and pseudo-first order, respectively. In addition, the results of response surface methodology (RSM) designed with biochar dose, reaction time, and benzene concentration showed the maximum adsorption capacity (ca. 136 mg BZ/g BC) similar to that from kinetic study. KB-BCs obtained as waste grass biomass may be a valuable adsorbent, and RSM may be a useful tool for the investigation of optimal conditions and results.

Keywords: biochar; benzene; adsorption; response surface methodology; Kentucky bluegrass

1. Introduction

The development of industry has led to environmental contamination caused by the release of various pollutants into the water and air. Volatile organic compounds (VOCs), organic compounds which have boiling points ranging from 50 to 260 °C at room temperature and under atmospheric pressure, also can lead to environmental pollution and have harmful effects on human health [1]. Benzene is one of the aromatic VOCs exhausted from diverse sources (e.g., paints, cosmetics, synthetic rubbers, glues, and other commodities) and has properties of low polarity and hydrophobicity [2]. Benzene is known as an environmental pollutant and a carcinogen in human. Additionally, chronic exposure to benzene can affect vital systems in the body, including the cardiovascular, nervous, reproductive, endocrine, respiratory, and immune systems [3]. Therefore, it is necessary to have a proper method for removing benzene.

There are several techniques for the removal of VOCs, include membrane separation, condensation, adsorption, absorption, and oxidation, etc. [4–7]. Among these environmental remediation methods, adsorption is a commonly used method for separating VOCs due to its efficiency and cost-effectiveness [8]. Several adsorbents are commonly used in commercial applications, such as synthetic resins, carbon nanostructures, zeolites, and

activated carbons [8–12]. However, commercially available adsorbents are expensive, energy intensive, and non-biodegradable [13]. In particular, carbonic materials (e.g., carbon nanotubes, graphene oxide, activated carbon, etc.) with remarkable adsorption ability are unsuitable to use widely because they demand complicated processes and high cost to fabricate as adsorbents. Since adsorbents play a key role in the adsorption of VOCs, there is still a need for cost-effective and eco-friendly improvements. Thus, biomass-based materials have received attention as novel adsorbents because they possess biodegradable, recyclable, eco-friendly properties along with varied characteristics that support the adsorption of pollutants.

Recently, biochar is considered as an efficient and economical alternative carbon material for various pollutant removal, such as VOCs, heavy metals, dyes, pharmaceuticals, and antibiotics [14–18]. Biochar is produced from various waste biomasses such as crops, lignocellulosic, seaweeds, algae, sewage sludge, manure, etc., via the pyrolysis process under O_2-limited conditions [15,17,19–23]. It has different physicochemical properties depending on the feedstock type and pyrolysis conditions (i.e., temperature, residence time, and heating rate) [20]. Moreover, the various characteristics of biochar, such as specific surface area, mineral content, functional groups, porous structure, etc., affect the mechanisms of pollutant removal. With its own characteristics, biochar has been widely used in environmental applications such as soil remediation, wastewater treatment, and water treatment [24–26]. In addition, research on the adsorption of VOCs by biochar has been growing rapidly in recent years [4]. According to Zhang et al., the adsorption capacity of VOCs (acetone, cyclohexane, and toluene) on biochar is influenced by the surface area of biochar, and physical adsorption and partitioning play a major role in the adsorption of VOCs on biochar [18]. Xiang et al. also reported that hickory wood-derived biochar, which is ball-milled, was effective for adsorption of VOCs (acetone, ethanol, chloroform, cyclohexane, and toluene) [27]. Kumar et al. tested the sorption of VOCs (carbon tetrachloride, chloroform, methyl chloride, benzene, toluene, and xylene) on unmodified biochar derived from various feedstocks and found that VOC removal is affected by feedstock material and pyrolysis temperature [28].

The efficiency of pollutant removal using adsorbents is influenced by various factors, including the duration of adsorption, the quantity of adsorbents, and the concentration of pollutants. Thus, optimizing the adsorption process is necessary for effective adsorption, and to obtain an optimized process, it is important to keep the independent variable constant while changing other parameters. The response surface methodology (RSM), which is a mathematical and statistical method, is widely used for process optimization in various fields including pollutants adsorption. This method is an analysis method that assumes a multivariate model between independent variables and response to find the optimal conditions of the experiments. By using this technique, it is possible to decrease the number of experiments, resulting in reduction of the experimental time, the material, and the labor force [29,30]. The Box–Behnken design is one of the most widely used RSMs that is a spherical and rotatable or nearly rotatable design. The design includes a central point and the middle points of the edges of the cube [31]. The Box–Behnken design is a type of quadratic multivariate design that is based on three-level incomplete factorial design [15]. Thus, for the adsorption of pollutants on biochar, which is influenced by many variables, the use of RSM is a suitable approach to optimize the adsorption conditions [15,32,33].

The main aim of this study is to evaluate the mechanism of benzene adsorption on the biochar using the isotherm and kinetic models. The possible mechanisms will be investigated according to the results of optimal biochar physicochemical properties, which will be analyzed by FTIR, ICP-OES, XRD, and XPS. Moreover, there were rapidly optimized benzene adsorption conditions on biochar using the Box–Behnken design of response surface methodology (RSM), which applied a biochar dose (0.002, 0.006, and 0.010 g), reaction time (2, 7, and 12 h), and benzene concentration (100, 200, and 300 ppm).

2. Materials and Methods

2.1. Chemicals

Benzene (hereafter, BZ), acetonitrile, and distilled water for HPLC grade were purchased from Sigma-Aldrich (St. Louis, MO, USA) and used to figure out the adsorption capacity onto biochar (BC) without further purification.

2.2. Preparation of BCs

The waste biomasses (rice husk: RH, Kentucky bluegrass: KB, and grape pomace: GP) as a feedstock for biochar production were used for the BZ adsorption experiment in the current study. As elucidated in the previous study, these feedstocks were dried and then ground. These feedstock-derived biochars were created in a Tube Furnace (OTF-1200X-S, MTI Co., Ltd., Richmond, CA, USA) at different pyrolytic temperatures (i.e., 350, 550, and 750 °C) for 2 h. The produced biochars were named corresponding to feedstock name and pyrolytic temperature (e.g., RH-BC350, RH-BC550, RH-BC750, KB-BC350, KB-BC550, KB-BC750, GP-BC350, GP-BC550, and GP-BC750).

2.3. Analysis of Biochar Properties

The specific surface areas (SSAs) of biochar were determined from N_2 adsorption isotherms at 77 K with a surface area analyzer (TriStarII, Micromeritics, Norcross, GA, USA). FTIR spectra were determined at a wavelength range between 600 and 4000 cm^{-1} by FTIR (FT/IR-4600, Jasco, Tokyo, Japan) for KB-BCs. X-ray diffraction (XRD) spectra were obtained using Rigaku SmartLab (Rigaku Co., Ltd., Tokyo, Japan) at 40 kV, and the data collection was conducted in the range of 2–80°. Mineral contents of N, P, K, Ca, Mg, and Fe were analyzed by ICP-OES (iCAP7400 DUO, Thermo Fisher Scientific, Waltham, MA, USA). The binding energy of compositions on the surface of KB-BC550 before and after BZ adsorption was investigated using X-ray photoelectron spectroscopy (XPS, K-Alpha, Thermo Scientific, Waltham, MA, USA).

2.4. Adsorption Experiments of Benzene

The batch adsorption experiments for BZ were conducted in 5 mL vials each containing a 4.5 mL BZ stock solution and 0.005 g of BC (i.e., GP-BCs, KB-BCs, and RH-BCs) to choose the best biochar. The stock solutions of BZ (200 mg/L) were prepared to evaluate the BZ adsorption capacity. All adsorption experiments were carried out at 20 °C with shaking (200 rpm) for 2 days with headspace minimization. After then, the supernatants were filtered to determine the adsorption capacity with 0.45 μm PVDF syringe filter (Whatman, Maidstone, UK). The adsorption capacity of BZ was determined following Equation (1):

$$\text{Adsorption capacity } (Q_e) = (C_0 - C_i) \times V/W, \tag{1}$$

where Q_e is the amount of BZ adsorbed onto the biochar (mg/g); C_0 and C_i are the initial and final BZ concentration (mg/L), respectively; V is the volume of the BZ solution (L); W is the amount of biochar (g).

The BZ removal efficiency was determined following Equation (2):

$$\text{Removal efficiency } (\%) = (A - B)/A \times 100, \tag{2}$$

where A is the initial concentration of BZ and B is the final concentration of BZ after the adsorption experiment.

The isotherm studies for BZ were conducted in 5 mL vials each containing a 4.5 mL BZ stock solution (300 mg/L) with 0.003 g BC–0.03 g BC (i.e., 0.003, 0.004, 0.005, 0.01, 0.015, 0.02, and 0.03 g BC) for 24 h. Moreover, the kinetic studies were carried out in 5 mL vials each containing a 4.5 mL BZ stock solution (300 mg/L) with 0.005 g BC for 12 h (i.e., measured at 60, 120, 240, 360, 480, 600, and 720 min). All adsorption experiments were carried out at 20 °C with shaking (200 rpm), and the supernatants were filtered to determine the adsorption capacity with 0.45 μm PVDF syringe filter (Whatman, Maidstone,

UK). The isotherm and kinetic models were calculated following equations as shown in Table S1.

2.5. Analytical Determination

BZ concentration was determined with high-performance liquid chromatography (HPLC, YL9100, Younglin Co., Ltd., Anyang, Republic of Korea) equipped with a YMC-Triart C18 column (150 × 4.6 mm, I.D. S-5 µm) and a UV detector at a wavelength of 254 nm. For BZ analysis, 60% analytical acetonitrile and 40% analytical pure water were used as the mobile phase at a flow rate of 1 mL/min.

2.6. RSM Design and Statistical Analysis

Response surface methodology (RSM) analysis was conducted using the Box–Behnken design, and the parameters (i.e., quantity of biochar (g), concentration of benzene (mg/L), and reaction time (hour)) for BZ adsorption capacity were evaluated to compare between optimal conditions and isotherm and kinetic studies. The main factors and levels were followed: quantity of biochar (g) (X_1), concentration of benzene (mg/L) (X_2), and reaction time (h) (X_3) as summarized in Table 1. The data were evaluated to fit a second-order polynomial model by Equation (3):

$$Y = \beta_0 + \sum_{i=1}^{k} \beta_i X_i + \sum_{i=1}^{k} \beta_{ii} X_i^2 + \sum_{i=1}^{k} \sum_{j=1}^{k} \beta_{ij} X_i X_j + \varepsilon \tag{3}$$

where Y is adsorption capacity of BZ; β_0, β_i (i = 1, 2, 3), β_{ii} (i = 1, 2, 3), and β_{ij} (i = 1, 2, 3; j = 1, 2, 3) are the various coefficients, while X_i and X_j are coded independent variables. The data were analyzed by Minitab 16.0 software (Minitab inc., State College, PA, USA).

Table 1. Coded and actual values of the various variables (quantity of biochar, concentration of benzene, reaction time) used in the Box–Behnken design.

Factor	Variables	Levels of Variables		
		−1	**0**	**+1**
X_1	Quantity of biochar (g)	0.002	0.006	0.01
X_2	Concentration of benzene (mg/L; ppm)	100	200	300
X_3	Reaction time (h)	2	7	12

3. Results and Discussion

3.1. Characterization and Screening of Biochar

To select the best biochar for BZ adsorption, prior to optimization of BZ adsorption conditions onto biochar, the specific surface area (SSA) and BZ adsorption capacity of the produced biochars (GP-BCs, KB-BCs, and RH-BCs) were evaluated, as shown in Figure 1. The adsorption capacity of biochar for BZ was in the following order: KB-BC > RH-BC > GP-BC. In the case of the SSA of biochar, the SSA of GP-BC increased with enhanced pyrolysis temperature, whereas the SSA of KB-BC and RH-BC showed a similar tendency to increase until 550 °C and then decrease. This result may be due to the structure stability of raw materials. Generally, high pyrolysis temperature induces the formation of pores in biochar structure; however, the porous structure is collapsed and is blocked with tar, resulting in SSA decrease [34]. The KB-BC and RH-BC produced at 550 °C possessed the highest BZ adsorption capacity (68.05 and 28.50 mg BZ/g BC) with the highest SSA (KB-BC550: 190.4 m^2/g, RH-BC550: 205.6 m^2/g) compared to those of others (KB-BC350, KB-BC750, RH-BC350, and RH-BC750), which were produced at 350 °C and 750 °C. In contrast, GP-BC produced at 750 °C revealed the highest BZ adsorption capacity (24.28 mg BZ/g BC) with the highest SSA (137.3 m^2/g) (Figure S1). These results indicate that the surface area partially affects BZ adsorption onto biochar, although there was no correspondence, perfectly. In the previous literature, the surface properties (e.g., functional groups,

specific surface area, pore size, and pore volume) of biochar correlated with the adsorption of aromatic compounds [35]. However, RH-BC350 with low SSA exhibited similar BZ adsorption capacity to GP-BC having high SSA, while KB-BC350 showed higher adsorption capacity. This result is attributed to the fact that the properties of biochar are influenced not only by the pyrolysis conditions but also by the type of raw biomass used [36,37]. Based on these results, KB-BC550, which had the highest BZ adsorption capacity, was chosen to evaluate a rapid optimization of the adsorption conditions and mechanisms between adsorbent and adsorbate.
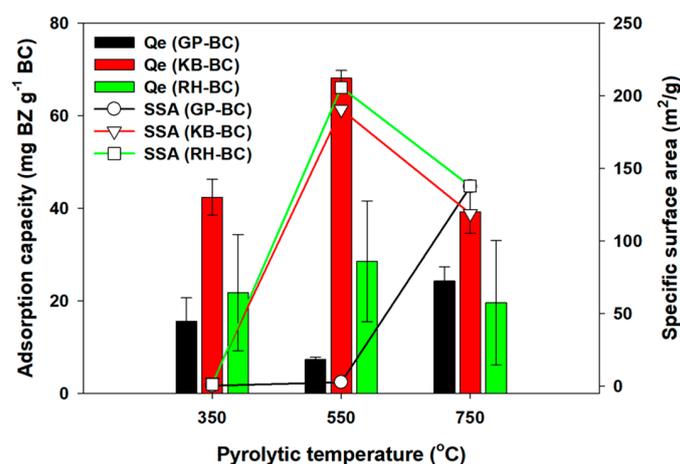
Figure 1. Comparison of adsorption capacity (Q_e) and specific surface area (SSA) of different biochars (GP−BCs, KB−BCs, and RH−BCs) produced at different pyrolytic temperatures (350 °C, 550 °C, and 750 °C). [Conditions] For benzene, 4.5 mL of 200 ppm; 0.005 g BC; initial pH of 7; 48 h. The experiments were conducted in triplicate.

The FTIR spectra, XRD spectra, and mineral compositions of KB-BCs were investigated as shown in Figure S2A–C. The FTIR spectra of feedstock and KB-BCs showed CO_3^{2-} (875 cm^{-1}), stretching vibration of C-O-C (1100 cm^{-1}), C-H bending (1430 cm^{-1}), aromatic conjugated C=O, C=C (1640 cm^{-1}), C=O stretching of carboxyl (1724 cm^{-1}), CH stretching of CH_2 and CH_3 (2930 cm^{-1}), and -OH (3200–3400 cm^{-1}) [34,38–40]. Among the KB-BCs, KB-BC550 lost various functional groups, including C-H bending, C=O stretching of carboxyl, CH stretching of CH_2 and CH_3, and -OH. In addition, most functional groups of KB-BC750 were eliminated. The functional groups on the surface of biochar were removed with the increase in pyrolytic temperature, as is well known [41]. When the pyrolysis temperature increased, dehydration, decarboxylation, decarbonylation, dehydrogenation, and demethanation occurred, leading to the decline of functional groups of biochar [36]. As shown in Figure S2B, the XRD spectra of KB-BC750 corresponding to SiO_2, $Ca(OH)_2$, and $CaCO_3$ at 2θ 26°, 28°, and 30°, respectively, revealed that higher pyrolysis temperature induced crystallization structure, owing to mineral concentration compared with KB-BC350 and KB-BC550 [34]. The mineral compositions of KB-BCs included N, P, K, Ca, Mg, and Fe. Among the minerals, the higher N content (2.0–2.6%) appeared in KB-BCs. However, N content decreased with the increase in pyrolytic temperature due to volatilization, while others increased. In the case of other minerals, the contents increased with the increase in pyrolytic temperature because minerals were concentrated [38,39,42]. This result accorded with the XRD analysis, which showed mineral enrichment of biochar at high pyrolysis temperature.

3.2. Isotherm Studies for Benzene Adsorption

The adsorbed BZ content onto the KB-BC550 improved with increasing biochar dosage (Figure 2), thereby the removal efficiency of KB-BC550 for BZ increased up to 94.9% when 0.03 g of biochar was added to the BZ solution.
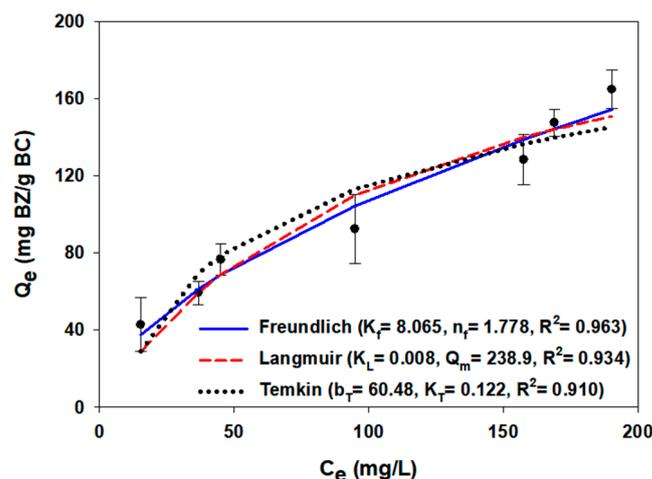
Figure 2. Isotherm studies of KB-BC550 for benzene adsorption by Langmuir, Freundlich, and Temkin isotherm models. [Conditions] For benzene, 4.5 mL of 300 ppm; 0.003–0.03 g BC (0.003, 0.004, 0.005, 0.01, 0.015, 0.02, 0.03 g); initial pH of 7; 24 h. The experiments were conducted in triplicate.

The BZ adsorption isotherm model studies containing Freundlich, Langmuir, and Temkin were assessed to compare to the results from RSM and evaluate adsorption potential of KB-BC550 in the present study. The Freundlich model, implying multilayer adsorption on the heterogeneous surface, was the best fitted, with higher R^2 (0.963) compared with others (i.e., Langmuir: R^2 = 0.934 and Temkin: R^2 = 0.910) (Figure 2 and Table S2). In addition, the Freundlich model was 1.778, indicating that the BZ adsorption process was physical adsorption [43]. Similar results, which suggest that the BZ and some compounds containing a BZ ring in their structure adsorb onto heterogeneous surface of biochar in multilayer through physisorption, were reported by researchers [44–47]. This result indicates that the adsorption ability of KB-BC550 for BZ was influenced by its surface area, which corresponds to the result that the adsorption capacity of KB-BCs was enhanced with increasing of SSA, as shown in Figure 1 [47]. According to many studies, the pore structure and SSA of porous carbon-based adsorbents are relevant to VOCs adsorption. In a study by Li et al., the pore structure of carbon materials affected the BZ adsorption, but the functional groups containing oxygen and nitrogen had no implication on the adsorption property for BZ [48]. Huang et al. also presented that the porous structure of biochar modified with $ZnCl_2$ led to a preferable environment for BZ adsorption [49]. The activated biochar prepared from wheat straw using the ball milling method showed enhanced BZ adsorption capacity with increasing specific surface area compared with untreated biochar [50].

3.3. Kinetic Studies for Benzene Adsorption

To evaluate the adsorption mechanism between BZ and KB-BC550, kinetic models including pseudo-first-order, pseudo-second-order, Elovich, two-compartment first-order, liquid film diffusion, and intra-particle diffusion models were applied in this study. As shown in Figure 3, the pseudo-first-order model (R^2 = 0.954) was the better fitted model for BZ adsorption onto KB-BC550, with higher R^2 value (>0.95) and lower SSE than the pseudo-second-order model. This result indicates that the BZ adsorption on KB-BC550 occurred through physisorption. The calculated Q_e value in the pseudo-first-order model was also closer to the experimental Q_e value than that of the pseudo-second-order model (Table S3). Additionally, the rate constants K_1 and K_2 showing less than 1 suggest that BZ was very rapidly adsorbed onto biochar [51]. The two-compartment first-order model was also suited for the BZ adsorption mechanism, with a high R^2 value (>0.95). As shown in Figure 3 and Table S3, the rapid adsorption of BZ in a few hours and the higher K_{fast} value than the K_{slow} value supported that fast adsorption was the dominant process. Moreover, the higher R^2 value (>0.94) of the liquid film diffusion model than the intra-particle diffusion model means that liquid film diffusion was a rate-controlling step.
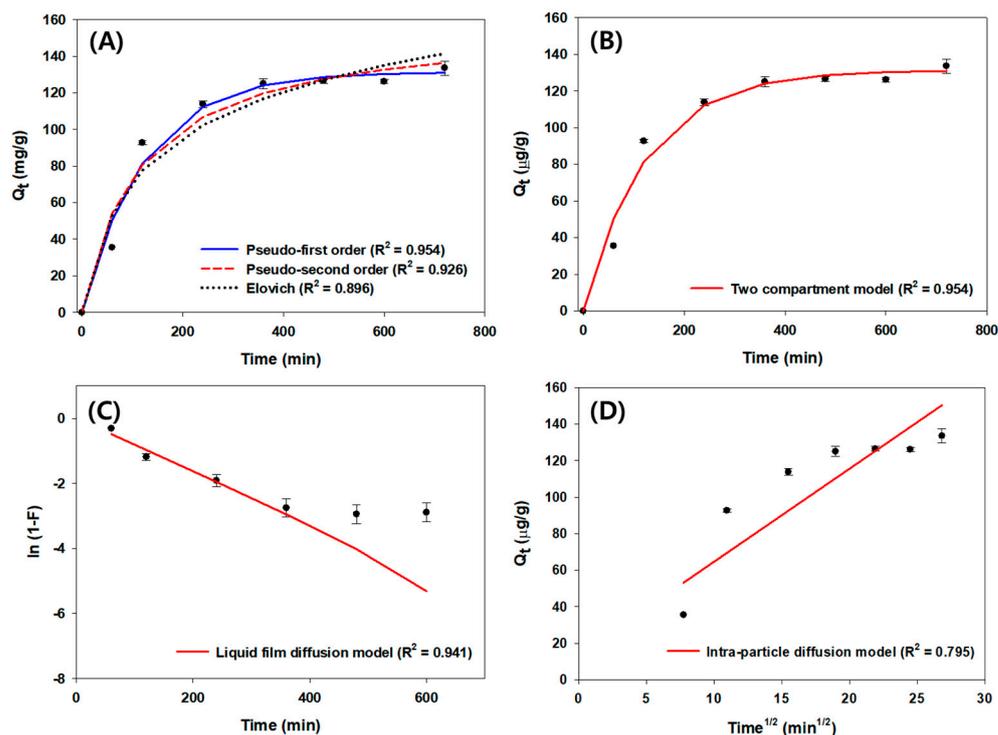
Figure 3. Kinetic studies of KB-BC550 for benzene adsorption by fitting pseudo−first−order, pseudo−second−order, and Elovich model (**A**), two−compartment model (**B**), liquid film diffusion model (**C**), and intra−particle diffusion model (**D**). [Conditions] For benzene, 4.5 mL of 300 ppm; 0.005 g BC; initial pH of 7; 1–12 h (60, 120, 240, 360, 480, 600, 720 min). The experiments were conducted in triplicate.

However, numerous research works have shown that the adsorption of compounds with a benzene ring (e.g., ethylbenzene, toluene, xylene, etc.) on carbon-based materials such as activated carbons, biochars, carbon nanotubes, graphenes, etc., followed the pseudo-second-order model more than the pseudo-first-order model [52–55]. These results may be due to differences in surface properties of carbonic materials depending on the adsorbent production method.

3.4. Possible Mechanisms for Benzene Adsorption onto KB-BC550

As exposed in Figure 1, the BZ adsorption increased with the increase in SSA, which implied that the SSA of biochar affected the BZ adsorption in relation to the pore-filling mechanism. The pore filling depends on the pore size of the biochar, with higher porosity containing a large number of active centers [56,57].

To compare the composition of KB-BC550 before and after BZ adsorption, XPS analysis was conducted. As shown in Figure 4, the survey scan of KB-BC550 revealed the peaks corresponding to Mg1s, O1s, K2s, K2p, C1s, and P2p [15,34,58,59]. In several peaks, there were changes in their peak intensities after BZ adsorption. The C1s peak at 285 eV indicating a C-C of a benzene ring had increased intensity, whereas the signals for P2p, K2s, and K2p were decreased. The P2p peak at 134 eV indicating the C-O-P peak decreased after BZ adsorption [60]. In addition, the K2p peak, which exhibited a doublet structure at 293 and 296 eV, disappeared at 293 eV, owing to the π-π* transition affiliated with the C1s. These results suggest that BZ adsorbed on KB-BC550 through π-π interactions (π-π stacking and π-π electron donor–acceptor interaction) between KB-BC550 and BZ [22,34,59,61].

Furthermore, the oxygen functional groups such as CO_3^{2-}, C=O, C=C, COOH, etc., as displayed in the FTIR spectrum of KB-BC550, propose interaction with BZ via hydrogen bonding [62]. According to the previously published studies, adsorption of organic pollutants is influenced by the surface properties of biochar, with the dominant mechanisms

being electrostatic attraction, π–π interaction, hydrogen bonding, and pore filling, which are associated with surface electrical properties, organic structure, and surface functional groups [1,37].
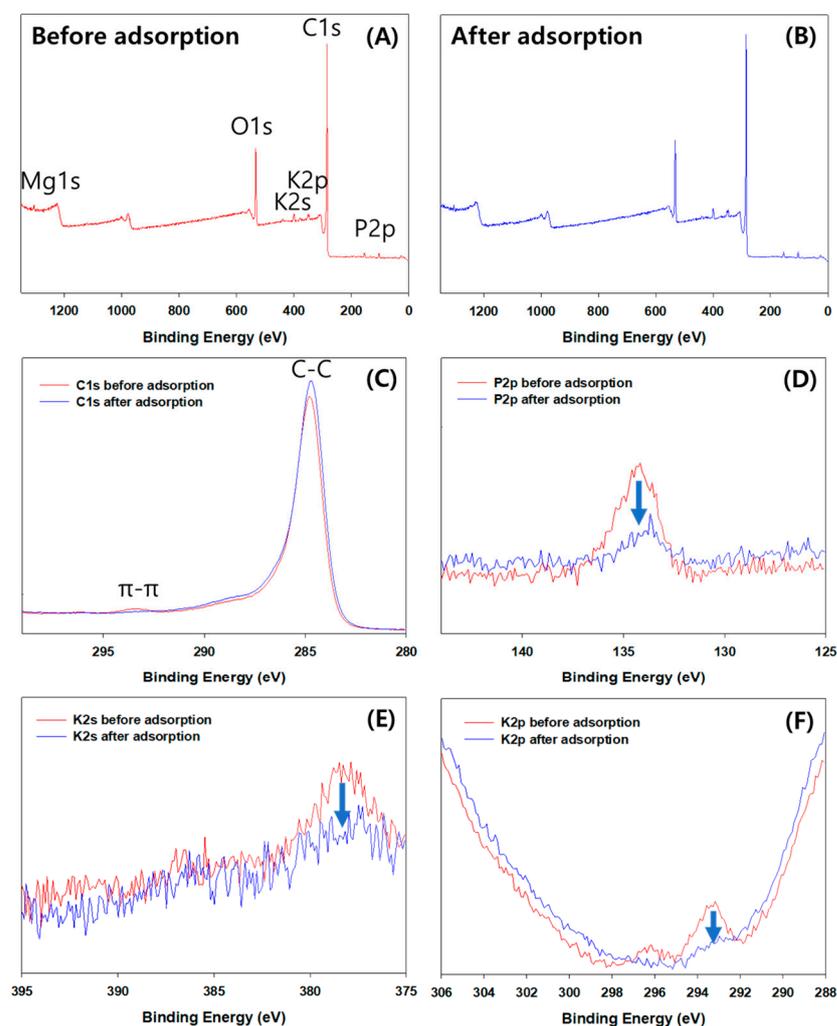

Figure 4. XPS survey scan (**A**,**B**), C1s (**C**), P2p (**D**), K2s (**E**), and K2p (**F**) of KB-BC550 before and after benzene adsorption. Arrow means the decrease of peak.

3.5. Effects of Biochar Dose, Concentration of Benzene, and Reaction Time on Adsorption Capacity from RSM Results

The biochar dose (0.002, 0.006, and 0.010 g), reaction time (2, 7, and 12 h), and BZ concentration (100, 200, and 300 ppm) were performed to investigate and optimize via response surface design (i.e., Box–Behnken) the effects of BZ adsorption capacity onto KB-BC550. The two-dimensional (2D) contour plots and responses (BZ adsorption capacity and removal efficiency) were shown in Figure 5a–c and Table S4. The BZ concentration, reaction time, and biochar dose influenced the BZ adsorption capacity. In particular, the BZ adsorption capacity was facilitated with the increase in BZ concentration and reaction time at around 0.006 g of biochar dose. The effects of these variables on the BZ adsorption capacity may cause the limited active sites on the surface of biochar and rate of transfer to reach equilibrium state. As shown in Table S4, the higher BZ adsorption capacity (143.92 mg BZ/g BC) appeared at 0.006 g biochar dose and 300 ppm BZ concentration for 12 h. Based on the experimental results summarized in Table S4, the predicted values for optimal adsorption capacity are shown in Figure 6. The 0.005 g biochar dose, 300 ppm BZ concentration, and 12 h of reaction time were predicted as the optimal conditions for maximum BZ adsorption capacity onto KB-BC550, indicating 136.80 mg BZ/g BC and

equilibrium state. According to the pseudo-first-order model, when the adsorbent dose, adsorbate concentration, and reaction time were 0.005 g, 300 ppm, and 8 h, respectively, the adsorption capacity of KB-BC550 was calculated to be 131.3 mg/g, which is similar to the RSM result. These consequences reveal that although RSM is unable to investigate adsorption mechanisms, it can be applied to deduce the optimal conditions and results of the adsorption process. Therefore, by using this technique, it is possible to decrease the number of experiments, resulting in reduction of the experimental time, the material, and the labor force.
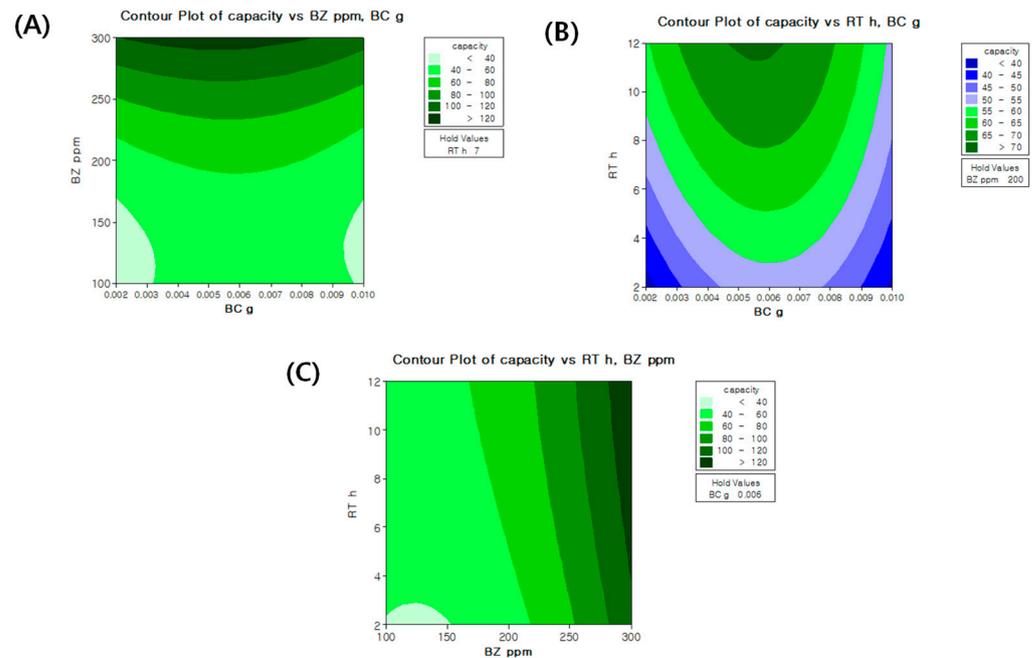
Figure 5. Two-dimensional contour plots showing effects of KB-BC550 dose (g), reaction time (RT, h), and benzene concentration (ppm) on adsorption capacity of benzene (BZ) (**A–C**).
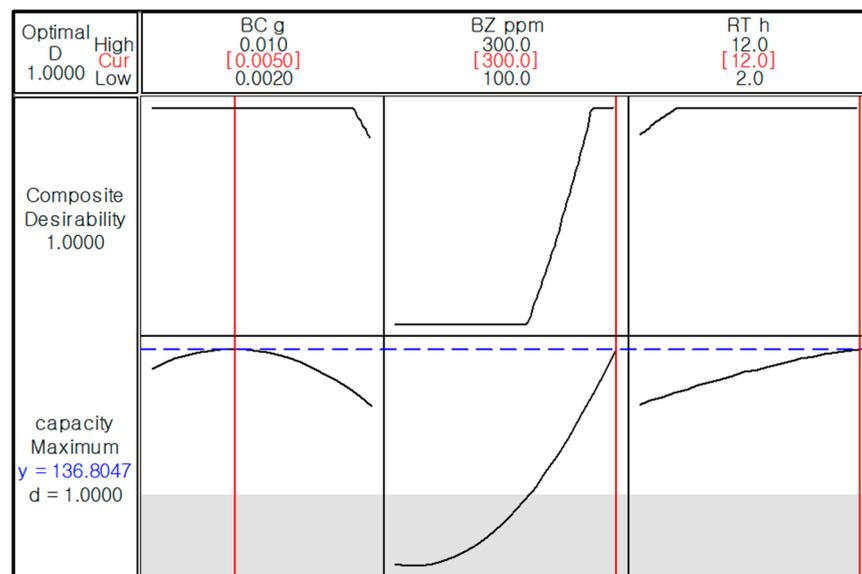
Figure 6. Predicted values of different variables (KB-BC550 dose (g), reaction time (RT, h), and benzene concentration (ppm)) for optimum adsorption capacity. Blue line is the chosen conditions for the optimum adsorption capacity of benzene. Red line is the optimal conditions of variables.

4. Conclusions

In this work, rice husk, Kentucky bluegrass, and grape pomace-derived biochars were prepared at different pyrolysis temperatures. Among the obtained biochars, KB-BC550 exhibited improving adsorption capacity for BZ due to higher SSA and functional groups compared to the other biochars. To analyze the adsorption mechanism, the adsorption isotherm and kinetic studies of KB-BC550 for BZ were conducted; consequently, it was found that Freundlich and pseudo-first order models meaning multilayered physical adsorption and heterogeneous surface adsorbent were suited to explain the BZ adsorption mechanism using KB-BC550. We also investigated optimal conditions and maximum adsorption capacity of KB-BC550 for BZ via RSM (Box–Behnken) and obtained similar results to the kinetic study. Thus, RSM may provide convenience for research by predicting adsorption conditions and results without isotherm and kinetic studies.

References

1. Shen, Y. Biomass-Derived Porous Carbons for Sorption of Volatile Organic Compounds (VOCs). *Fuel* **2023**, *336*, 126801. [CrossRef]
2. Vikrant, K.; Kim, K.H.; Peng, W.; Ge, S.; Sik Ok, Y. Adsorption Performance of Standard Biochar Materials against Volatile Organic Compounds in Air: A Case Study Using Benzene and Methyl Ethyl Ketone. *Chem. Eng. J.* **2020**, *387*, 123943. [CrossRef]
3. Bahadar, H.; Mostafalou, S.; Abdollahi, M. Current Understandings and Perspectives on Non-Cancer Health Effects of Benzene: A Global Concern. *Toxicol. Appl. Pharmacol.* **2014**, *276*, 83–94. [CrossRef] [PubMed]
4. Gan, G.; Fan, S.; Li, X.; Zhang, Z.; Hao, Z. Adsorption and Membrane Separation for Removal and Recovery of Volatile Organic Compounds. *J. Environ. Sci.* **2023**, *123*, 96–115. [CrossRef] [PubMed]
5. Gupta, V.K.; Verma, N. Removal of Volatile Organic Compounds by Cryogenic Condensation Followed by Adsorption. *Chem. Eng. Sci.* **2002**, *57*, 2679–2696. [CrossRef]
6. Darracq, G.; Couvert, A.; Couriol, C.; Amrane, A.; Thomas, D.; Dumont, E.; Andres, Y.; Le Cloirec, P. Silicone Oil: An Effective Absorbent for the Removal of Hydrophobic Volatile Organic Compounds. *J. Chem. Technol. Biotechnol.* **2010**, *85*, 309–313. [CrossRef]
7. Kamal, M.S.; Razzak, S.A.; Hossain, M.M. Catalytic Oxidation of Volatile Organic Compounds (VOCs)—A Review. *Atmos. Environ.* **2016**, *140*, 117–134. [CrossRef]
8. Li, X.; Zhang, L.; Yang, Z.; Wang, P.; Yan, Y.; Ran, J. Adsorption Materials for Volatile Organic Compounds (VOCs) and the Key Factors for VOCs Adsorption Process: A Review. *Sep. Purif. Technol.* **2020**, *235*, 116213. [CrossRef]
9. Liu, H.; Yu, Y.; Shao, Q.; Long, C. Porous Polymeric Resin for Adsorbing Low Concentration of VOCs: Unveiling Adsorption Mechanism and Effect of VOCs' Molecular Properties. *Sep. Purif. Technol.* **2019**, *228*, 115755. [CrossRef]

10. Zhang, X.; Gao, B.; Creamer, A.E.; Cao, C.; Li, Y. Adsorption of VOCs onto Engineered Carbon Materials: A Review. *J. Hazard. Mater.* **2017**, *338*, 102–123. [CrossRef]

11. Li, X.; Wang, J.; Guo, Y.; Zhu, T.; Xu, W. Adsorption and Desorption Characteristics of Hydrophobic Hierarchical Zeolites for the Removal of Volatile Organic Compounds. *Chem. Eng. J.* **2021**, *411*, 128558. [CrossRef]

12. Li, B.; Mi, C. On the Adsorption of Volatile Organic Compounds on Hydroxyl-Functionalized Carbon Nanotubes in Aqueous Solution. *Diam. Relat. Mater.* **2022**, *125*, 108994. [CrossRef]

13. Park, S.; Lee, J.W.; Kim, J.E.; Kang, G.; Kim, H.J.; Choi, Y.K.; Lee, S.H. Adsorptive Behavior of Cu^{2+} and Benzene in Single and Binary Solutions onto Alginate Composite Hydrogel Beads Containing Pitch Pine-Based Biochar. *Polymers* **2022**, *14*, 3468. [CrossRef] [PubMed]

14. Qiu, B.; Tao, X.; Wang, H.; Li, W.; Ding, X.; Chu, H. Biochar as a Low-Cost Adsorbent for Aqueous Heavy Metal Removal: A Review. *J. Anal. Appl. Pyrolysis* **2021**, *155*, 105081. [CrossRef]

15. Choi, Y.K.; Gurav, R.; Kim, H.J.; Yang, Y.H.; Bhatia, S.K. Evaluation for Simultaneous Removal of Anionic and Cationic Dyes onto Maple Leaf-Derived Biochar Using Response Surface Methodology. *Appl. Sci.* **2020**, *10*, 2982. [CrossRef]

16. Chauhan, S.; Shafi, T.; Dubey, B.K.; Chowdhury, S. Biochar-Mediated Removal of Pharmaceutical Compounds from Aqueous Matrices via Adsorption. *Waste Dispos. Sustain. Energy* **2023**, *5*, 37–62. [CrossRef] [PubMed]

17. Zhang, P.; Li, Y.; Cao, Y.; Han, L. Characteristics of Tetracycline Adsorption by Cow Manure Biochar Prepared at Different Pyrolysis Temperatures. *Bioresour. Technol.* **2019**, *285*, 121348. [CrossRef]

18. Zhang, X.; Gao, B.; Zheng, Y.; Hu, X.; Creamer, A.E.; Annable, M.D.; Li, Y. Biochar for Volatile Organic Compound (VOC) Removal: Sorption Performance and Governing Mechanisms. *Bioresour. Technol.* **2017**, *245*, 606–614. [CrossRef]

19. Saeed, A.A.H.; Harun, N.Y.; Sufian, S.; Siyal, A.A.; Zulfiqar, M.; Bilad, M.R.; Vagananthan, A.; Al-Fakih, A.; Ghaleb, A.A.S.; Almahbashi, N. Eucheuma Cottonii Seaweed-Based Biochar for Adsorption of Methylene Blue Dye. *Sustainability* **2020**, *12*, 10318. [CrossRef]

20. Janu, R.; Mrlik, V.; Ribitsch, D.; Hofman, J.; Sedláček, P.; Bielská, L.; Soja, G. Biochar Surface Functional Groups as Affected by Biomass Feedstock, Biochar Composition and Pyrolysis Temperature. *Carbon Resour. Convers.* **2021**, *4*, 36–46. [CrossRef]

21. Das, S.K.; Ghosh, G.K.; Avasthe, R. Conversion of Crop, Weed and Tree Biomass into Biochar for Heavy Metal Removal and Wastewater Treatment. *Biomass Convers. Biorefin.* **2023**, *13*, 4901–4914. [CrossRef]

22. Gurav, R.; Bhatia, S.K.; Choi, T.R.; Choi, Y.K.; Kim, H.J.; Song, H.S.; Lee, S.M.; Lee Park, S.; Lee, H.S.; Koh, J.; et al. Application of Macroalgal Biomass Derived Biochar and Bioelectrochemical System with Shewanella for the Adsorptive Removal and Biodegradation of Toxic Azo Dye. *Chemosphere* **2021**, *264*, 128539. [CrossRef]

23. Regkouzas, P.; Diamadopoulos, E. Adsorption of Selected Organic Micro-Pollutants on Sewage Sludge Biochar. *Chemosphere* **2019**, *224*, 840–851. [CrossRef]

24. Wang, J.; Wang, S. Preparation, Modification and Environmental Application of Biochar: A Review. *J. Clean Prod.* **2019**, *227*, 1002–1022. [CrossRef]

25. Enaime, G.; Baçaoui, A.; Yaacoubi, A.; Lübken, M. Biochar for Wastewater Treatment-Conversion Technologies and Applications. *Appl. Sci.* **2020**, *10*, 3492. [CrossRef]

26. Kamali, M.; Appels, L.; Kwon, E.E.; Aminabhavi, T.M.; Dewil, R. Biochar in Water and Wastewater Treatment—A Sustainability Assessment. *Chem. Eng. J.* **2021**, *420*, 129946. [CrossRef]

27. Xiang, W.; Zhang, X.; Chen, K.; Fang, J.; He, F.; Hu, X.; Tsang, D.C.W.; Ok, Y.S.; Gao, B. Enhanced Adsorption Performance and Governing Mechanisms of Ball-Milled Biochar for the Removal of Volatile Organic Compounds (VOCs). *Chem. Eng. J.* **2020**, *385*, 123842. [CrossRef]

28. Kumar, A.; Singh, E.; Khapre, A.; Bordoloi, N.; Kumar, S. Sorption of Volatile Organic Compounds on Non-Activated Biochar. *Bioresour. Technol.* **2020**, *297*, 122469. [CrossRef] [PubMed]

29. Anfar, Z.; Ait Ahsaine, H.; Zbair, M.; Amedlous, A.; Ait El Fakir, A.; Jada, A.; El Alem, N. Recent Trends on Numerical Investigations of Response Surface Methodology for Pollutants Adsorption onto Activated Carbon Materials: A Review. *Crit. Rev. Environ. Sci. Technol.* **2020**, *50*, 1043–1084. [CrossRef]

30. Baytar, O.; Şahin, Ö.; Horoz, S.; Kutluay, S. High-Performance Gas-Phase Adsorption of Benzene and Toluene on Activated Carbon: Response Surface Optimization, Reusability, Equilibrium, Kinetic, and Competitive Adsorption Studies. *Environ. Sci. Pollut. Res.* **2020**, *27*, 26191–26210. [CrossRef]

31. Tripathi, P.; Srivastava, V.C.; Kumar, A. Optimization of an Azo Dye Batch Adsorption Parameters Using Box-Behnken Design. *Desalination* **2009**, *249*, 1273–1279. [CrossRef]

32. Biswas, S.; Bal, M.; Behera, S.K.; Sen, T.K.; Meikap, B.C. Process Optimization Study of Zn^{2+} Adsorption on Biochar-Alginate Composite Adsorbent by Response Surface Methodology (RSM). *Water* **2019**, *11*, 325. [CrossRef]

33. Dissanayake Herath, G.A.; Poh, L.S.; Ng, W.J. Statistical Optimization of Glyphosate Adsorption by Biochar and Activated Carbon with Response Surface Methodology. *Chemosphere* **2019**, *227*, 533–540. [CrossRef] [PubMed]

34. Song, H.J.; Gurav, R.; Bhatia, S.K.; Lee, E.B.; Kim, H.J.; Yang, Y.H.; Kan, E.; Kim, H.H.; Lee, S.H.; Choi, Y.K. Treatment of Microcystin-LR Cyanotoxin Contaminated Water Using Kentucky Bluegrass-Derived Biochar. *J. Water Process Eng.* **2021**, *41*, 102054. [CrossRef]

35. Tan, X.F.; Zhu, S.S.; Wang, R.P.; Chen, Y.D.; Show, P.L.; Zhang, F.F.; Ho, S.H. Role of Biochar Surface Characteristics in the Adsorption of Aromatic Compounds: Pore Structure and Functional Groups. *Chin. Chem. Lett.* **2021**, *32*, 2939–2946. [CrossRef]

36. Chen, Y.; Zhang, X.; Chen, W.; Yang, H.; Chen, H. The Structure Evolution of Biochar from Biomass Pyrolysis and Its Correlation with Gas Pollutant Adsorption Performance. *Bioresour. Technol.* **2017**, *246*, 101–109. [CrossRef] [PubMed]

37. Dai, Y.; Zhang, N.; Xing, C.; Cui, Q.; Sun, Q. The Adsorption, Regeneration and Engineering Applications of Biochar for Removal Organic Pollutants: A Review. *Chemosphere* **2019**, *223*, 12–27. [CrossRef] [PubMed]

38. Choi, Y.K.; Kan, E. Effects of Pyrolysis Temperature on the Physicochemical Properties of Alfalfa-Derived Biochar for the Adsorption of Bisphenol A and Sulfamethoxazole in Water. *Chemosphere* **2019**, *218*, 741–748. [CrossRef]

39. Kim, J.E.; Bhatia, S.K.; Song, H.J.; Yoo, E.; Jeon, H.J.; Yoon, J.Y.; Yang, Y.; Gurav, R.; Yang, Y.H.; Kim, H.J.; et al. Adsorptive Removal of Tetracycline from Aqueous Solution by Maple Leaf-Derived Biochar. *Bioresour. Technol.* **2020**, *306*, 123092. [CrossRef]

40. Liu, L.; Liu, G.; Zhou, J.; Wang, J.; Jin, R.; Wang, A. Improved Bioreduction of Nitrobenzene by Black Carbon/Biochar Derived from Crop Residues. *RSC Adv.* **2016**, *6*, 84388–84396. [CrossRef]

41. Wang, Z.; Cao, J.; Wang, J. Pyrolytic Characteristics of Pine Wood in a Slowly Heating and Gas Sweeping Fixed-Bed Reactor. *J. Anal. Appl. Pyrolysis* **2009**, *84*, 179–184. [CrossRef]

42. Özçimen, D.; Ersoy-Meriçboyu, A. Characterization of Biochar and Bio-Oil Samples Obtained from Carbonization of Various Biomass Materials. *Renew. Energy* **2010**, *35*, 1319–1324. [CrossRef]

43. Sadegh, F.; Sadegh, N.; Wongniramaikul, W.; Apiratikul, R.; Choodum, A. Adsorption of Volatile Organic Compounds on Biochar: A Review. *Process Saf. Environ. Prot.* **2024**, *182*, 559–578. [CrossRef]

44. Fan, X.; Wang, X.; Zhao, B.; Wan, J.; Tang, J.; Guo, X. Sorption Mechanisms of Diethyl Phthalate by Nutshell Biochar Derived at Different Pyrolysis Temperature. *J. Environ. Chem. Eng.* **2022**, *10*, 107328. [CrossRef]

45. Jayawardhana, Y.; Mayakaduwa, S.S.; Kumarathilaka, P.; Gamage, S.; Vithanage, M. Municipal Solid Waste-Derived Biochar for the Removal of Benzene from Landfill Leachate. *Environ. Geochem. Health* **2019**, *41*, 1739–1753. [CrossRef] [PubMed]

46. Jayawardhana, Y.; Kumarathilaka, P.; Mayakaduwa, S.; Weerasundara, L.; Bandara, T.; Vithanage, M. Characteristics of Municipal Solid Waste Biochar: Its Potential to Be Used in Environmental Remediation. In *Utilization and Management of Bioresources*; Springer: Singapore, 2018; pp. 209–220. [CrossRef]

47. Xiao, L.; Bi, E.; Du, B.; Zhao, X.; Xing, C. Surface Characterization of Maize-Straw-Derived Biochars and Their Sorption Performance for MTBE and Benzene. *Environ. Earth Sci.* **2014**, *71*, 5195–5205. [CrossRef]

48. Li, D.; Su, R.; Ma, X.; Zeng, Z.; Li, L.; Wang, H. Porous Carbon for Oxygenated and Aromatic VOCs Adsorption by Molecular Simulation and Experimental Study: Effect Pore Structure and Functional Groups. *Appl. Surf. Sci.* **2022**, *605*, 154708. [CrossRef]

49. Huang, Y.; Chu, H.; Wang, D.; Hui, S. Performance and Mechanism of Benzene Adsorption on $ZnCl_2$ One-Step Modified Corn Cob Biochar. *Environ. Sci. Pollut. Res.* **2024**, *31*, 15209–15222. [CrossRef] [PubMed]

50. Qi, G.; Pan, Z.; Zhang, X.; Miao, X.; Xiang, W.; Gao, B. Effect of Ball Milling with Hydrogen Peroxide or Ammonia Hydroxide on Sorption Performance of Volatile Organic Compounds by Biochar from Different Pyrolysis Temperatures. *Chem. Eng. J.* **2022**, *450*, 138027. [CrossRef]

51. Zeng, S.; Choi, Y.K.; Kan, E. Iron-Activated Bermudagrass-Derived Biochar for Adsorption of Aqueous Sulfamethoxazole: Effects of Iron Impregnation Ratio on Biochar Properties, Adsorption, and Regeneration. *Sci. Total Environ.* **2021**, *750*, 141691. [CrossRef]

52. Bakather, O.Y. Adsorption of Benzene on Impregnated Carbon Nanotubes. *Ain Shams Eng. J.* **2020**, *11*, 905–912. [CrossRef]

53. da Costa Lopes, A.S.; de Carvalho, S.M.L.; do Socorro Barros Brasil, D.; de Alcântara Mendes, R.; Lima, M.O. Surface Modification of Commercial Activated Carbon (CAG) for the Adsorption of Benzene and Toluene. *Am. J. Anal. Chem.* **2015**, *06*, 528–538. [CrossRef]

54. Jayawardhana, Y.; Keerthanan, S.; Lam, S.S.; Vithanage, M. Ethylbenzene and Toluene Interactions with Biochar from Municipal Solid Waste in Single and Dual Systems. *Environ. Res.* **2021**, *197*, 111102. [CrossRef] [PubMed]

55. Raad, M.T.; Behnejad, H.; Jamal, M. El Equilibrium and Kinetic Studies for the Adsorption of Benzene and Toluene by Graphene Nanosheets: A Comparison with Carbon Nanotubes. *Surf. Interface Anal.* **2016**, *48*, 117–125. [CrossRef]

56. Hassan, M.; Liu, Y.; Naidu, R.; Parikh, S.J.; Du, J.; Qi, F.; Willett, I.R. Influences of Feedstock Sources and Pyrolysis Temperature on the Properties of Biochar and Functionality as Adsorbents: A Meta-Analysis. *Sci. Total Environ.* **2020**, *744*, 140714. [CrossRef] [PubMed]

57. Qiu, B.; Shao, Q.; Shi, J.; Yang, C.; Chu, H. Application of Biochar for the Adsorption of Organic Pollutants from Wastewater: Modification Strategies, Mechanisms and Challenges. *Sep. Purif. Technol.* **2022**, *300*, 121925. [CrossRef]

58. Cui, Q.; Xu, J.; Wang, W.; Tan, L.; Cui, Y.; Wang, T.; Li, G.; She, D.; Zheng, J. Phosphorus Recovery by Core-Shell γ-Al_2O_3/Fe_3O_4 Biochar Composite from Aqueous Phosphate Solutions. *Sci. Total Environ.* **2020**, *729*, 138892. [CrossRef] [PubMed]

59. Smith, M.W.; Pecha, B.; Helms, G.; Scudiero, L.; Garcia-Perez, M. Chemical and Morphological Evaluation of Chars Produced from Primary Biomass Constituents: Cellulose, Xylan, and Lignin. *Biomass Bioenergy* **2017**, *104*, 17–35. [CrossRef]

60. Luo, Y.; Li, R.; Sun, X.; Liu, X.; Li, D. The Roles of Phosphorus Species Formed in Activated Biochar from Rice Husk in the Treatment of Landfill Leachate. *Bioresour. Technol.* **2019**, *288*, 121533. [CrossRef]

61. Tong, Y.; McNamara, P.J.; Mayer, B.K. Adsorption of Organic Micropollutants onto Biochar: A Review of Relevant Kinetics, Mechanisms and Equilibrium. *Environ. Sci.* **2019**, *5*, 821–838. [CrossRef]
62. Wu, C.H.; Chang, S.H.; Lin, C.W. Improvement of Oxygen Release from Calcium Peroxide-Polyvinyl Alcohol Beads by Adding Low-Cost Bamboo Biochar and Its Application in Bioremediation. *Clean* **2015**, *43*, 287–295. [CrossRef]